Acta Mechanica 97, 153–168 (1993)

ACTA MECHANICA

Effect of frictional force on the steady state axisymmetric deformations of a viscoplastic target

X. Chen and **R. C. Batra,** Rolla, Missouri

(Received November 5, 1991; revised January 17, 1992)

Summary. We study steady state axisymmetric deformations of a thick viscoplastic target being penetrated by a fast-moving long rigid cylindrical rod with a hemispherical nose. The deformations of the target appear steady to an observer situated on the penetrator nose tip and moving with it. The objective of this work is to investigate the effect of the frictional force acting on the target/penetrator interface upon the deformations of the target. It is postulated that the frictional force at a point on the target/penetrator interface is proportional to the normal traction there and depends upon the speed of the target particle relative to the penetrator. It is found that the frictional force affects significantly the variation of the tangential speed and the second invariant of the strain-rate tensor on the penetrator nose surface, but minimally the distribution of the normal stress there, since the dominant component of the normal stress is the hydrostatic pressure which is affected little by the consideration of friction forces.

1 Introduction

In previous papers [1]–[6], Batra and co-workers have studied in detail the penetration problem in which the fast moving rod is assumed to be semi-infinite and the target infinite with a semi-infinite hole, and the rate of penetration and all flow fields are steady as seen from the nose of the penetrator. They examined the effect of different nose shapes and flow rules used to model the viscoplastic response of the target and penetrator materials. Here we relax their assumption of the target/penetrator interface being smooth and study in some detail the effect of considering frictional forces at the target/penetrator interface. We resolve the difficult question of modelling the friction force by first motivating that it should depend upon the relative speed of the two sliding surfaces and the normal traction between them. An approximate value of the two constants appearing in the expression for the frictional force is determined by comparing the distribution of the frictional force on the penetrator nose surface obtained from a solution of the penetration problem with that found by modelling the steady state penetration process as a viscous fluid flowing around the rigid penetrator. The fluid flow results in a thin boundary layer abutting the penetrator surface. We recall that Birkhoff et al. [7] and Pack and Evans [8] described the hypervelocity impact by a modified Bernoulli equation in which material strength was represented as a resistive pressure. Alekseevskii [9] and Tate [10] considered separate resistive pressures for the target and the penetrator. Tate [11] has recently given expressions for these resistive pressures in terms of Young's modulus and the flow stress of the material.

For a review of the open literature on ballistic penetration, we refer the reader to Backman and Goldsmith [12], Jones and Zukas [13], and Anderson and Bodner [14]. Engineering models of ballistic penetration have been proposed by Awerbuch [15], Awerbuch and Bodner [16], Ravid and Bodner [17], Ravid et al. [18], Batra and Chen [19], Jones et al. [20], Woodward [21], and Forrestal et al. [22].

The work described herein is in the spirit of our previous work [1] – [6], initiated a few years ago by Batra and Wright [3], with the hope that the kinematic and stress fields reported herein will help in devising and/or checking results from simpler engineering theories of penetration.

2 Formulation of the problem

We use cylindrical coordinates with the origin attached to the penetrator nose tip and z-axis pointing into the penetrator to describe the axisymmetric deformations of a viscoplastic target. Recalling that the penetrator is moving at a steady speed, equations governing the target deformations and written in terms of non-dimensional variables are

$$\operatorname{div} \boldsymbol{v} = 0, \tag{1}$$

$$\operatorname{div} \boldsymbol{\sigma} = \alpha(\boldsymbol{v} \cdot \operatorname{grad})\, \boldsymbol{v}, \tag{2}$$

$$\boldsymbol{\sigma} = -p\boldsymbol{1} + \frac{(1 + bI)^m}{\sqrt{3}\, I}\, \boldsymbol{D}, \tag{3}$$

$$2\boldsymbol{D} = \operatorname{grad} \boldsymbol{v} + (\operatorname{grad} \boldsymbol{v})^T, \tag{4}$$

$$2I^2 = \operatorname{tr}(\boldsymbol{D}^2). \tag{5}$$

Here $\boldsymbol{v}$ is the velocity of a target particle relative to the penetrator, $\boldsymbol{\sigma}$ is the Cauchy stress tensor, p is the hydrostatic pressure not determined by the deformation history, $\boldsymbol{D}$ is the strain-rate tensor, the material parameters b and m characterize the strain-rate sensitivity of the material, $\alpha = \varrho_t v_0^2/\sigma_0$ is a non-dimensional number that signifies the importance of inertia forces relative to the flow stress of the material, ϱ_t is the mass density of the target material, v_0 the steady penetration speed, and σ_0 is the flow stress of the target material in a quasistatic simple tension or compression test. The non-dimensional variables are related to the dimensional variables denoted below by a superimposed bar as follows:

$$\begin{aligned} &\boldsymbol{v} = \bar{\boldsymbol{v}}/v_0, \quad \boldsymbol{\sigma} = \bar{\boldsymbol{\sigma}}/\sigma_0, \quad p = \bar{p}/\sigma_0, \quad r = \bar{r}/r_0, \quad z = \bar{z}/r_0, \\ &\boldsymbol{I} = \bar{\boldsymbol{I}}\frac{r_0}{v_0}, \quad \boldsymbol{D} = \bar{\boldsymbol{D}}\frac{r_0}{v_0}. \end{aligned} \tag{6}$$

Henceforth we work in terms of non-dimensional variables.

Equation (1) and that obtained by substituting from (3), (4), and (5) into (2), subject to appropriate boundary conditions, are to be solved for p and $\boldsymbol{v}$. We seek an approximate solution of these coupled nonlinear partial differential equations by the finite element method, which necessitates that we consider a finite target region. The target region studied and its discretization into finite elements is depicted in Fig. 1. For the boundary conditions, we take

$$\boldsymbol{t} \cdot \boldsymbol{\sigma n} = g(\boldsymbol{v}, \boldsymbol{n} \cdot \boldsymbol{\sigma n}) \quad \text{on the target/penetrator interface } \Gamma_i, \tag{7.1}$$

$$\boldsymbol{v} \cdot \boldsymbol{n} = 0 \quad \text{on } \Gamma_i, \tag{7.2}$$

$$\sigma_{zz} = 0, \quad v_r = 0 \quad \text{on the bounding surface AB}, \tag{7.3}$$

$$v_r = 0, \quad v_z = -1.0 \quad \text{on the bounding surface EFA}, \tag{7.4}$$

$$\sigma_{rz} = 0, \quad v_r = 0 \quad \text{on the axis of symmetry DE}. \tag{7.5}$$

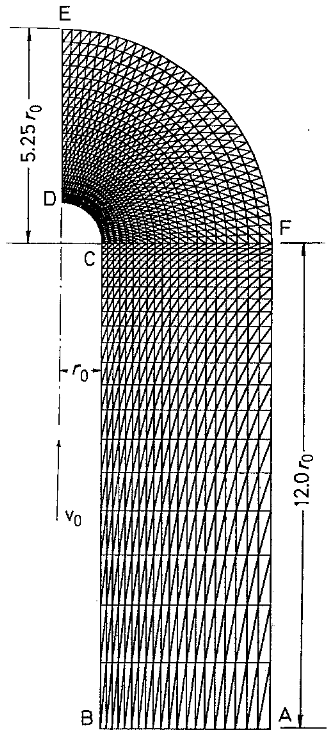

Fig. 1. The finite region analyzed and its discretization

Here $\boldsymbol{n}$ and $\boldsymbol{t}$ denote, respectively, a unit normal and a unit vector tangent to the surface, and Γ_i is the surface DCB. The boundary condition (7.1) implies that the tangential force at a point on the target/penetrator interface is a function of the relative velocity and normal traction there. Oden et al. [23] have motivated such a form for the frictional force. It has also been used by Chen [24] in studying the penetration of a rigid ogival nosed cylindrical projectile into a geological target. We discuss the specific form of the frictional force a little later. The boundary condition (7.2) signifies that there is no penetration of a target particle into the penetrator. The boundary conditions (7.3) and (7.4) are good approximations, provided that the target region studied is large. One way to ensure the adequacy of the region analyzed is to study the problem for successively larger regions till the solution variables at target particles near the target/penetrator interface change within desirable tolerances. The boundary conditions (7.5) follow from the assumption that the target deformations are axisymmetric.

With the definitions

$$f_t \equiv \boldsymbol{t} \cdot \boldsymbol{\sigma n}, \quad f_n \equiv \boldsymbol{n} \cdot \boldsymbol{\sigma n}, \tag{8}$$

we rewrite (7.1) as

$$f_t = g(\boldsymbol{v}, f_n). \tag{9}$$

We note that there is no failure criterion for the target material included in our work.

2.1 *Hypothesis for the frictional force*

We assume that the frictional force at a point on Γ_i is proportional to the normal traction there and opposes the motion of the target particle relative to the penetrator. That is,

$$f_t = -\upsilon f_n \boldsymbol{e}_v, \quad \boldsymbol{e}_v \equiv \boldsymbol{v}/|\boldsymbol{v}|. \tag{10}$$

In Coulomb's law, υ is taken as a constant and the frictional force is independent of the magnitude of the relative velocity of sliding between the two bodies. That Coulomb's law is not appropriate for the present problem can be realized by considering the state of stress at the stagnation point D in Fig. 1. Recalling the boundary condition (7.5), i.e., $\sigma_{rz} = 0$, and the symmetry of the Cauchy stress tensor, we see that $f_t = \sigma_{zr} = 0$ at point D. However, $f_n \neq 0$ there. Rather, f_n is expected to be maximum at the stagnation point D.

We postulate that the frictional force f_t is continuously distributed on Γ_i, and take

$$\upsilon = \mu v^{\beta}, \tag{11.1}$$

obtaining thereby

$$\boldsymbol{f}_t = -\mu v^{\beta} f_n \boldsymbol{e}_v, \tag{11.2}$$

where $v = (v_r^2 + v_z^2)^{1/2}$ is the magnitude of $\boldsymbol{v}$, and μ and β are constants. For Coulomb's law, $\beta = 0$. We note that

$$\upsilon = \upsilon_\infty + (\upsilon_0 - \upsilon_\infty)\, e^{-\gamma v} \tag{12}$$

assumed by Chen [24] satisfies $\boldsymbol{f}_t = \boldsymbol{0}$ at the stagnation point D only when $\upsilon_0 = 0$. In Eq. (12), υ_0, υ_∞ and γ are constants. Equation (11.2) is valid for a certain range, to be determined experimentally, of values of v. Here we assume it to hold for moderate penetration speeds considered in this study.

2.2 *Determination of parameters in the friction law*

In order to determine an approximate value of β in Eq. (11), we envisage that the target material flowing around the penetrator can be regarded as a fluid, somewhat akin to the solenoidal fluid flow model of Tate [25]. At a large distance from the penetrator nose tip, the fluid can be regarded as nonviscous or perfect, and the fluid viscosity plays a dominant role in a thin layer surrounding the penetrator. With respect to the orthogonal curvilinear coordinate axes (x, y) shown in Fig. 2, a general momentum integral that gives the shearing traction τ_0 at a point on the hemispherical nose surface of the penetrator can be written as [26]

$$\tau_0 = \varrho_f \left[U^2 \frac{d\theta^*}{dx} + (2\theta^* + \delta^*)\, U \frac{dU}{dx} + U^2 \frac{\theta^*}{r} \frac{dr}{dx} \right], \tag{13}$$

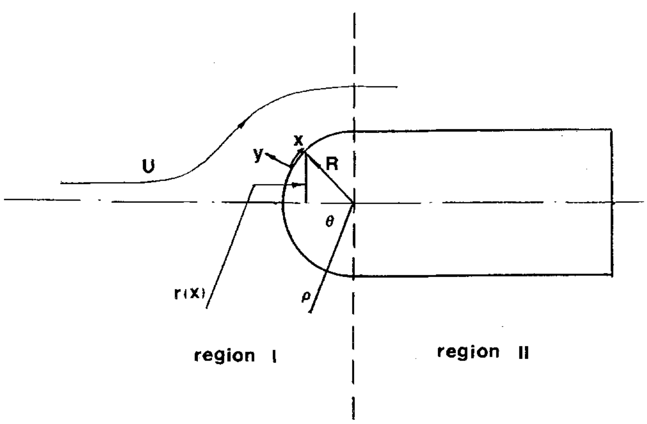

Fig. 2. Schematic sketch of the fluid flow around the penetrator, and the coordinate systems used

where

$$\delta^* = \int_0^\infty \left(1 - \frac{u}{U}\right) dy, \tag{14.1}$$

$$\theta^* = \int_0^\infty \frac{u}{U}\left(1 - \frac{u}{U}\right) dy, \tag{14.2}$$

$$\tau_0 = \mu_f \left.\frac{\partial u}{\partial y}\right|_{y=0}, \tag{14.3}$$

u and U denote, respectively, the x-velocity of a fluid particle within the boundary layer and at far away points, ϱ_f is the mass density, and μ_f the shear viscosity of the fluid. We make the Karman-Pohlhausen [26] approximation, i.e.,

$$u = U(a + \hat{b}\eta + c\eta^2 + d\eta^3 + e\eta^4), \tag{15.1}$$

where

$$\eta = y/\delta(x), \tag{15.2}$$

$\delta(x)$ is the thickness of the boundary layer, and $a, \hat{b}, c, d$, and e are constants to be determined from the following boundary conditions:

$$\begin{gathered} u(x, 0) = 0, \quad u(x, \delta) = U(x), \\ \frac{\partial u}{\partial y}(x, \delta) = 0, \quad \frac{\partial^2 u}{\partial y^2}(x, \delta) = 0, \\ \frac{\partial^2 u}{\partial y^2}(x, 0) = -\varrho_f \frac{U(x)}{\mu_f}\frac{dU}{dx}. \end{gathered} \tag{16}$$

A solution of Eq. (15.1) under the boundary conditions (16) is

$$\frac{u}{U} = 1 - (1 + \eta)(1 - \eta)^3 + \frac{\lambda}{6}\eta(1 - \eta)^3, \tag{17.1}$$

where

$$\lambda \equiv \varrho_f \frac{\delta^2}{\mu_f}\frac{dU}{dx}. \tag{17.2}$$

With the definitions

$$\phi = \varrho_f \theta^{*2}/\mu_f, \tag{18.1}$$

$$\varkappa = \phi \frac{dU}{dx}, \tag{18.2}$$

the general momentum integral (13) can be written as

$$U \frac{d\phi}{dx} = H(\varkappa), \tag{19.1}$$

where

$$H(\varkappa) = 2[g(\varkappa) - (2 + f(\varkappa))\, \varkappa] - \frac{2}{r} \frac{dr}{dx} \frac{U}{U'}\, \varkappa, \qquad U' \neq 0, \tag{19.2}$$

$$= 2[g(\varkappa) - (2 + f(\varkappa))\, \varkappa] - \frac{2}{r} \frac{dr}{dx}\, U\phi, \qquad U' = 0, \tag{19.3}$$

$$g(\varkappa) = \left(2 + \frac{\lambda}{6}\right) h(\varkappa) = \frac{\tau_0}{U} \sqrt{\frac{\phi}{\varrho_f \mu_f}}, \tag{19.4}$$

$$f(\varkappa) = \left(\frac{3}{10} - \frac{\lambda}{120}\right) \Big/ h(\varkappa), \tag{19.5}$$

$$\varkappa(x) = \lambda h^2(\varkappa), \tag{19.6}$$

$$h(\varkappa) = \frac{37}{315} - \frac{\lambda}{945} - \frac{\lambda^2}{9072}. \tag{19.7}$$

We note that, because of Eq. (17.2), we have two unknowns, say $\varkappa$ and ϕ. The laminar boundary layer theory requires that $|\lambda| \leqq 12$. We determine the far field velocity U by studying the solutions of the steady state penetration problems analyzed earlier, in which the target/penetrator interface Γ_i was taken to be smooth. This is justified, since in the region away from the penetrator surface, the fluid is modelled as nonviscous, and the effect of the frictional force on the target/penetrator interface should be minimal there.

Batra and Chen [19] represented the velocity field in steady state penetration of a viscoplastic target by a hemispherical nosed rigid cylindrical penetrator as

$$v_\theta = \left(1 - \frac{1}{\varrho^{n+1}} + \frac{1}{\varrho^n}\right) \sin\theta + \sum_{m,k} C_{mk} \varrho^m \sin^k 2\theta, \tag{20.1}$$

$$\begin{aligned} v_\varrho = {} & \left[\left(\frac{1}{\varrho^2} - 1\right) \cos\theta - \frac{2}{1-n}\left(\frac{1}{\varrho^2} - \frac{1}{\varrho^{n+1}}\right) \cos\theta + \frac{2}{2-n}\left(\frac{1}{\varrho^2} - \frac{1}{\varrho^n}\right) \cos\theta\right] \\ & - \sum_{m,k} \frac{C_{mk}}{m+2}\left(\frac{1}{\varrho^2} - \varrho^m\right) \sin^{k-1} 2\theta((2k+1)\cos 2\theta + 1) \end{aligned} \tag{20.2}$$

in region I, and

$$v_z = -\left(1 - \frac{1}{r^{n+1}} + \frac{1}{r^n}\right), \qquad v_r = 0 \tag{21}$$

in region II. The constants n and C_{mk} were determined by ensuring that the error in integrating the balance of linear momentum was minimum. Regions I and II are identified in Fig. 2. Batra and Chen found that the solution computed with the leading term differed very little from that found by also including the next two terms in the series. Here we consider only the leading terms and assume that

$$U(x)\begin{cases}= \sin x & \text{in region I}, & (22.1)\\ = 1 & \text{in region II}. & (22.2)\end{cases}$$

At the stagnation point, $U(x) = 0$, and from Eq. (19.1),

$$H(\varkappa) = 0 \quad \text{at the stagnation point}. \tag{23}$$

The value of λ is determined from Eq. (23). Having found λ, all other solution variables can be computed there. The solution is marched forward in the x-direction by using the forward-difference method, and the shearing force at every point on the hemispherical nose surface can be found.

The steady state penetration problem defined by Eqs. (1) and (2), and boundary conditions (7) with the frictional force given by Eq. (11) was solved by the finite element method using the computer code developed by Batra [5]. The code was modified to include the frictional force on the target/penetrator interface. The code employs six-noded triangular elements with v_r and v_z approximated in each element by quadratic polynomials defined in terms of the values of v_r and v_z at the node points, and the pressure field approximated by a polynomial of degree one defined in terms of its values at the vertices of the triangle. The system of nonlinear algebraic equations was solved iteratively, until at each node point

$$\|\mathbf{v}^m - \mathbf{v}^{m-1}\| \leqq 0.02\,\|\mathbf{v}^{m-1}\|,$$

$$|p^m - p^{m-1}| \leqq 0.02\,|p^{m-1}|.$$

Material parameters in Eq. (3) were assigned values $b = 1.0 \times 10^6$ and $m = 0.09$. Thus, the target material is assumed to exhibit strong strain-rate hardening effects. Batra [4] has investigated the effect of the values of b and m on the deformations of the target.

The value of β was adjusted so that the peak value of the tangential force given by the finite element solution of the penetration problem with $\alpha = 15$ and the boundary layer theory occurred

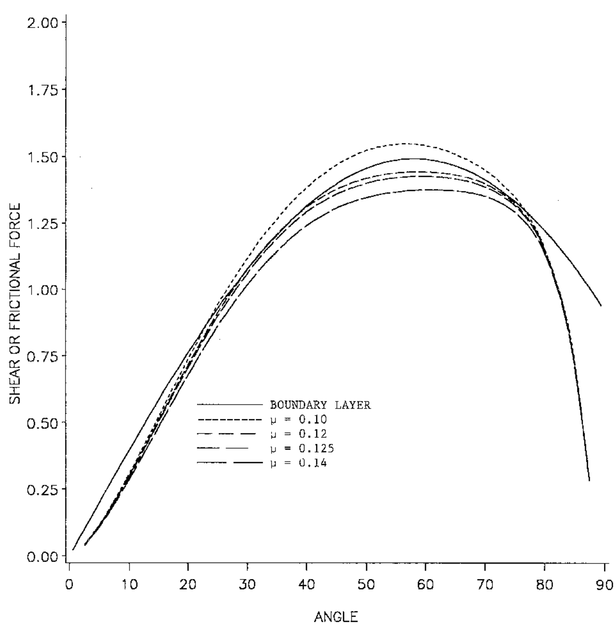

Fig. 3. A comparison of the distribution of the frictional force on the hemispherical nose of the penetrator as found from a solution of the penetration problem and the boundary layer theory

at nearly the same location on the penetrator nose surface. We note that for the solution given by the boundary layer theory, the peak value of the shear traction occurred at the same location for different values of Reynold's number or the fluid viscosity considered. A large value of α is taken here, since the validity of the boundary layer approximation improves with an increase in the fluid speed in the outer region. The value of μ was found so that the peaks in the two solutions were close to each other. This procedure resulted in

$$\mu \simeq 0.12, \quad \beta = 1.5,$$

and the two solutions are plotted in Fig. 3. The parameters ϱ_f and μ_f were assigned values so that the shearing tractions for the two methods had identical expressions in terms of non-dimensional variables. It is clear from the results plotted in Fig. 3 that the shear tractions are sensitive to the value of μ. Henceforth, we keep β fixed and compute results for the penetration problem for different values of μ.

3 Results for the penetration problem

3.1 Effect of different values of the coefficient of friction

Figure 4a depicts the distribution of the normal traction, f_n, on the hemispherical nose surface of the penetrator for $b = 1.0 \times 10^6$, $m = 0.09$, $\alpha = 6.15$, and $\mu = 0.0, 0.1, 0.2, 0.3$, and 0.4. Since the deviatoric stress $\boldsymbol{s}$ defined as

$$\boldsymbol{s} = \boldsymbol{\sigma} + p\boldsymbol{1}$$

satisfies

$$(\mathrm{tr}\, \boldsymbol{s}^2)^{1/2} = \sqrt{\frac{2}{3}}\,(1 + bI)^m,$$

a significant contribution to the value of f_n is made by the hydrostatic pressure, which seems to be less sensitive to the value of μ. Thus, the value and the distribution of normal tractions on the penetrator nose surface change very little when μ is increased from 0.0 to 0.4. Whatever little change does occur, the general trend is that f_n increases near the nose tip and decreases near the nose periphery with an increase in the value of μ. We have plotted the strain-rate measure I and the tangential speed on the nose surface for different values of μ in Figs. 4b and 4c, respectively. Near the nose tip, the strain-rate measure decreases noticeably with an increase in the value of μ, and it increases sharply at points close to the nose periphery with an increase in the value of μ. For $m = 0.09$, an increase in the value of I from 0.5 to 3.0 will enhance the value of f_n by a factor of 1.175. Even though I increases at points near the nose periphery, the resulting increase in the value of f_n is more than compensated for by a decrease in its value caused by the drop in the value of the hydrostatic pressure there. The plots in Fig. 4c reveal that the tangential speed changes significantly with an increase in the value of μ. Both the magnitude and the curvature of the curves are affected by the value of μ. These curves provide a partial explanation for the effect the value of μ has on the distribution of the strain-rate invariant at points on the nose surface.

The variation of $(-\sigma_{zz})$ and the strain-rate measure I on the axial line for $\mu = 0.0, 0.1, 0.2, 0.3$, and 0.4 is exhibited in Fig. 5. At target particles within a distance of $0.5r_0$ from the penetrator

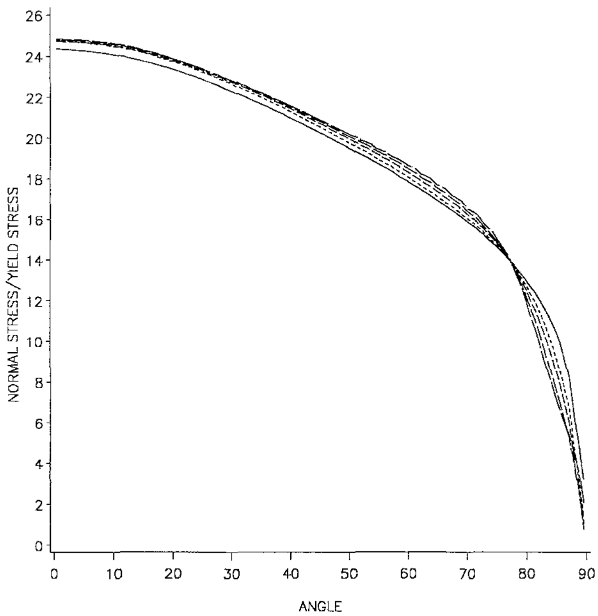

a

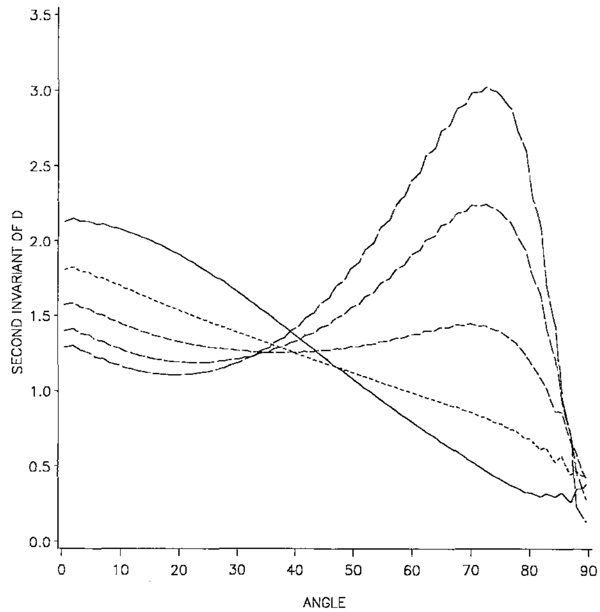

b

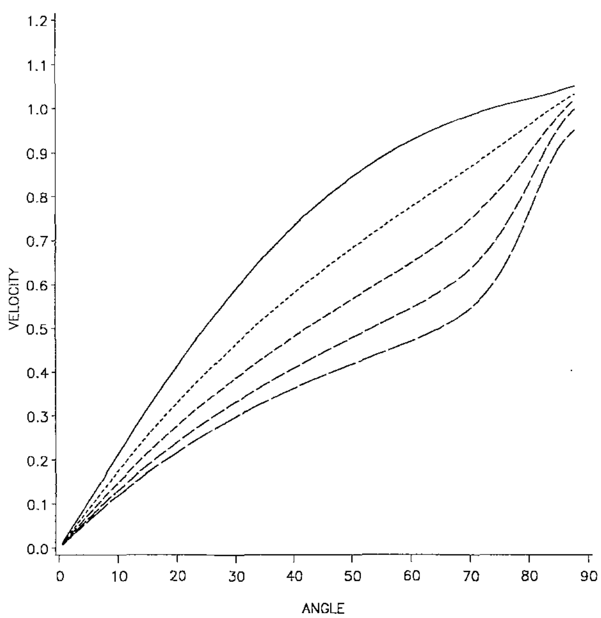

c

Fig. 4. Distribution of **a** the normal traction, **b** the strain-rate measure I, and **c** the tangential speed on the hemispherical nose of the penetrator for different values of the coefficient of friction (——— $\mu = 0.0$, --------- $\mu = 0.1$, – – – – $\mu = 0.20$, — — — — $\mu = 0.3$, — — — — $\mu = 0.4$)

nose tip, the values of the strain-rate measure I decrease significantly with an increase in the value of μ. This change is less noticeable in the value of σ_{zz} because it is dominated by the value of the hydrostatic pressure. Values of I drop rather quickly, signifying that severe deformations of the target occur within a distance of $3r_0$ from the target/penetrator interface. Assuming that the target material is high strength steel for which $\varrho_0 = 7\,800$ kg/m^3 and $\sigma_0 = 400$ MPa, we obtain $v_0 = 562$ m/s for $\alpha = 6.15$. Thus, the nondimensional values of I need to be multiplied by nearly 10^5 to get their dimensional counterparts.

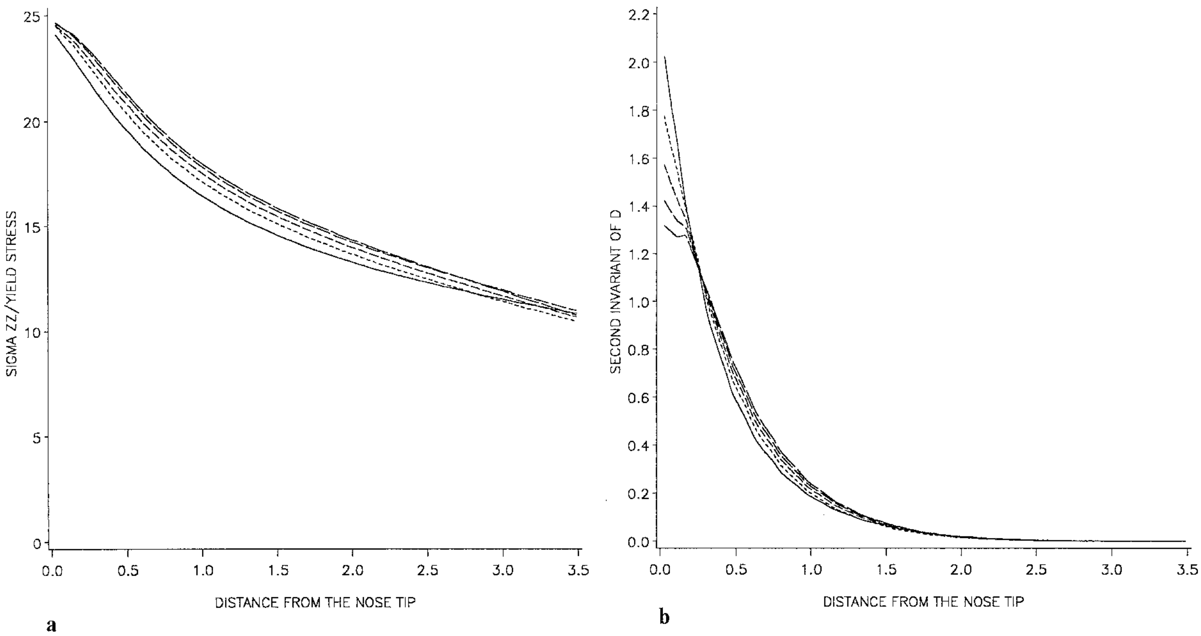

Fig. 5. Variation of $-\sigma_{zz}$ and the strain-rate measure I on the axial line for different values of the coefficient of friction (see Fig. 4 for the legend to the curves)

The dependence of the axial resisting force experienced by the penetrator upon the coefficient of friction μ is plotted in Fig. 6. Note that the tangential tractions acting on the penetrator nose surface do have a component in the axial direction, and thus retard the motion of the penetrator. Thus, even though the normal tractions depend rather weakly upon μ, the dependence of the axial resisting force F upon μ is moderate. We note that the dimensional values of the axial resisting force are obtained by multiplying their nondimensional values by $(\pi r_0{}^2 \sigma_0)$.

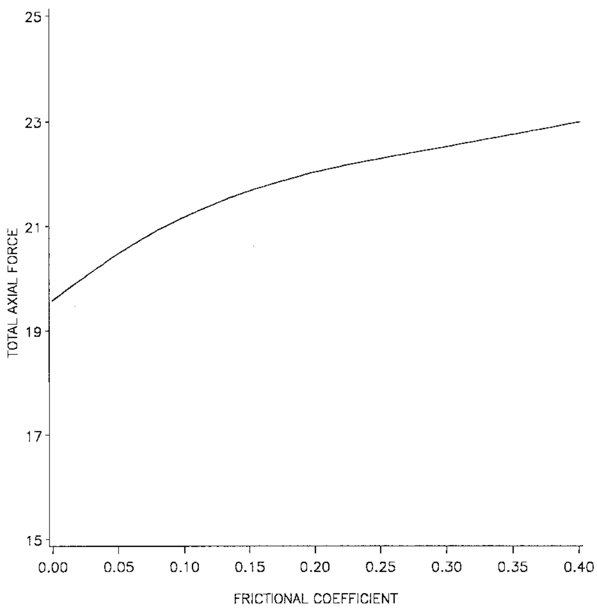

Fig. 6. Dependence of the axial resisting force experienced by the penetrator upon the coefficient of friction μ

3.2 Effect of penetration speed

For results presented in this Section, we take $\mu = 0.12$ and vary the penetration speed. In Figs. 7a and 7b, we have plotted the distribution of the normal traction, the second invariant of the strain-rate tensor $\boldsymbol{D}$, and the tangential speed on the penetrator nose surface for $\alpha = 6, 8, 10, 12$, and 15. As for the case when the target/penetrator interface was taken to be smooth, the normal tractions around the nose tip increase with α, those at points adjacent to the nose periphery decrease with α, and the normal tractions at $\theta = 45°$ remain unaffected by the value of α. A similar trend is exhibited by the values of the second invariant I of the strain-rate tensor $\boldsymbol{D}$. The tangential speed is zero at the stagnation point and increases to one at the nose periphery. At

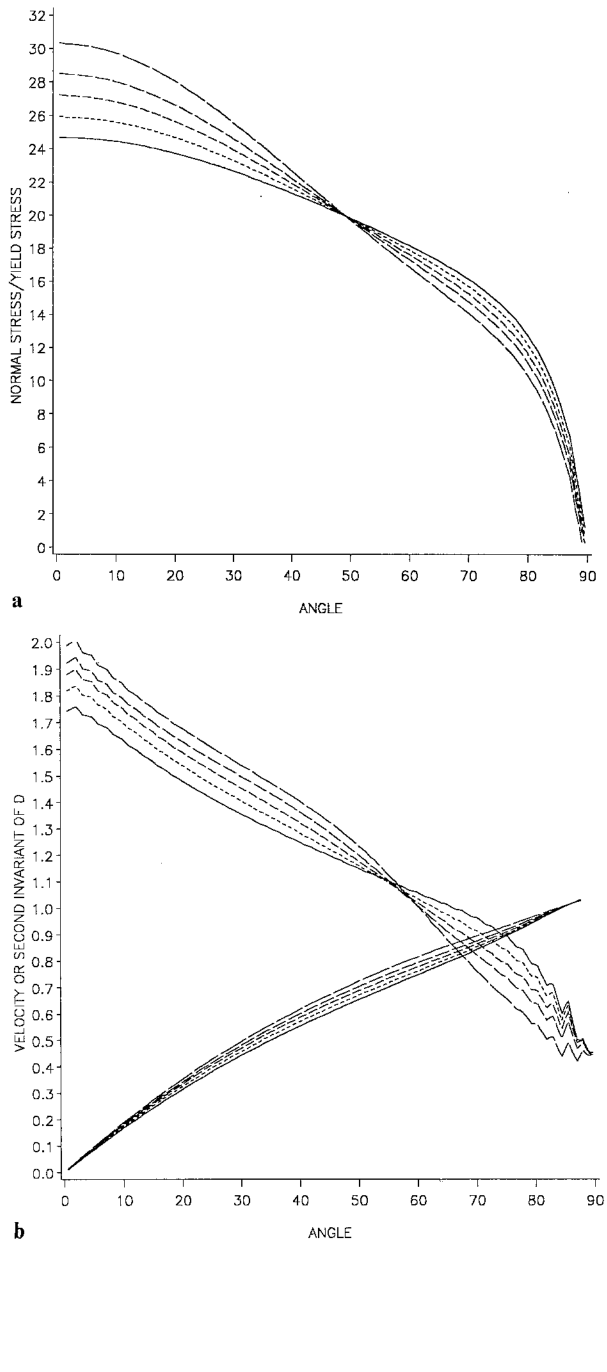

a

b

Fig. 7. Distribution of the normal traction, the second invariant of the strain-rate tensor, and the tangential speed on the penetrator nose surface for different values of α (——— $\alpha = 6$, ---------- $\alpha = 8$, ----- $\alpha = 10$, — — — — $\alpha = 12$, —— —— $\alpha = 15$)

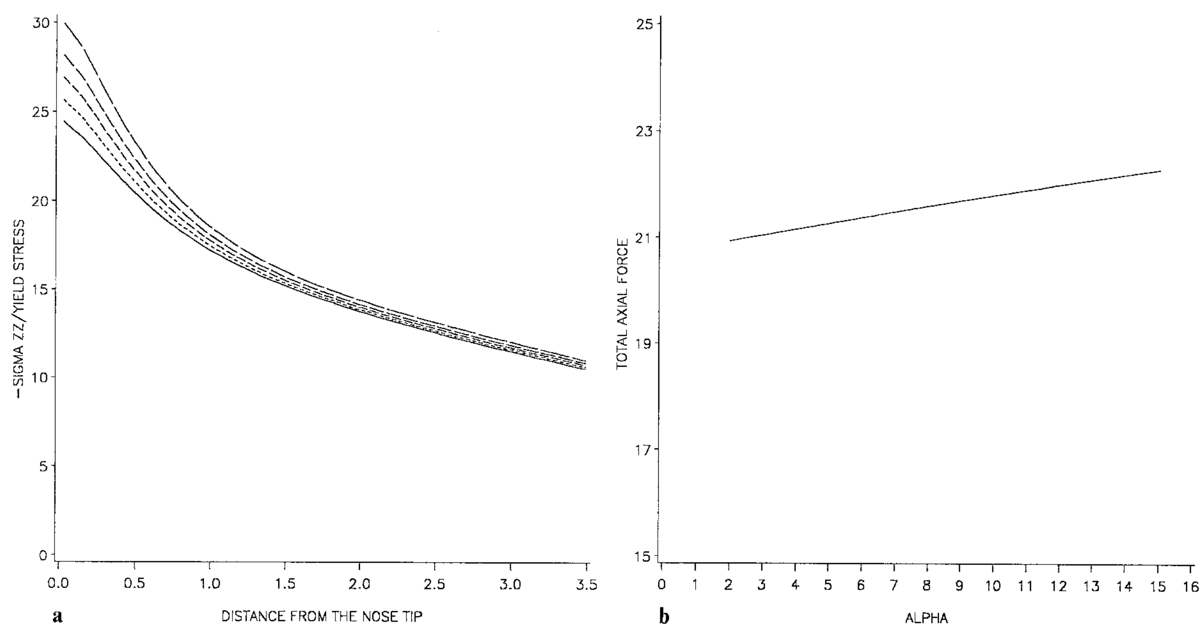

Fig. 8. **a** Dependence of $-\sigma_{zz}$ at points on the axial line upon α (see Fig. 7 for the legend to the curves) **b** Dependence of the axial resisting force experienced by the penetrator upon α

intermediate points, the tangential speed increases with an increase in α, but the change is not that large. Figures 8a and 8b depict, respectively, the variation of $(-\sigma_{zz})$ on the axial line for $\alpha = 6$, 8, 10, 12, and 15, and the dependence of the axial resisting force experienced by the penetrator upon α. As for the no-friction case, the dependence of the axial resisting force upon α is very weak. For all values of α considered, the magnitude of σ_{zz} at points on the axial line decays slowly as we move away from the penetrator nose tip, primarily because the hydrostatic pressure decreases slowly because of the resistance offered by the essentially non-deforming target material surrounding the severely deforming material around the penetrator nose. In [6], Jayachandran and Batra accounted for the elastic deformations of the target and found that $(-\sigma_{zz})$ dropped to one-fifth of its peak value at a distance of $4r_0$ from the nose tip. Here $(-\sigma_{zz})$ drops to nearly one-half of the peak value over the same distance.

3.3 Effect of penetrator nose shape

Figure 9 exhibits the distribution of the normal traction on the penetrator nose surface for three different nose shapes, viz., blunt with $r_n/r_0 = 0.2$, hemispherical with $r_n/r_0 = 1.0$, and ellipsoidal with $r_n/r_0 = 2.0$. Here r_n and r_0 equal the semi-major and semi-minor axes of the penetrator nose. In each case, two values of μ, namely, 0.0 and 0.12, are considered and α was set equal to 8. The difference between the normal tractions for $\mu = 0.0$ and $\mu = 0.12$ is maximum for the ellipsoidal nosed penetrator and minimum for the blunt nosed penetrator. For each value of μ, the normal traction near the penetrator nose tip increases with an increase in the value of r_n/r_0, and the reverse happens near the nose periphery. The increase in the value of f_n near the nose tip is both due to an increase in the value of the second invariant of the strain-rate tensor and the hydrostatic

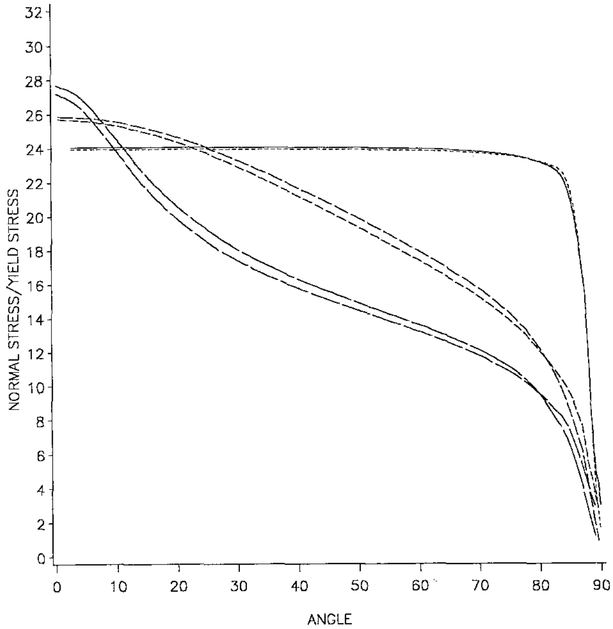

Fig. 9. Distribution of the normal traction on the penetrator nose surface for three different nose shapes both with and without the consideration of frictional forces (blunt nose, ——— $\mu = 0$, --------- $\mu = 0.12$; hemispherical nose, – – – – $\mu = 0.0$, — — — — $\mu = 0.12$; ellipsoidal nose, — — — — $\mu = 0.0$, ——— — — $\mu = 0.12$)

pressure there. As expected, for a blunt nosed penetrator the normal tractions stay essentially uniform over the nose surface and suddenly drop to zero at points adjacent to the nose periphery.

The distribution of the second invariant I of the strain-rate tensor $\boldsymbol{D}$ and the tangential speed on the penetrator nose surface for the three nose shapes and $\alpha = 8$ is plotted in Fig. 10. For the blunt nosed penetrator the strain-rate invariant I becomes very large near the nose periphery. For the other two nose shapes, the maximum value of I occurs near the nose tip. The effect of frictional force is to decrease slightly the value of I at every point on the nose surface. However,

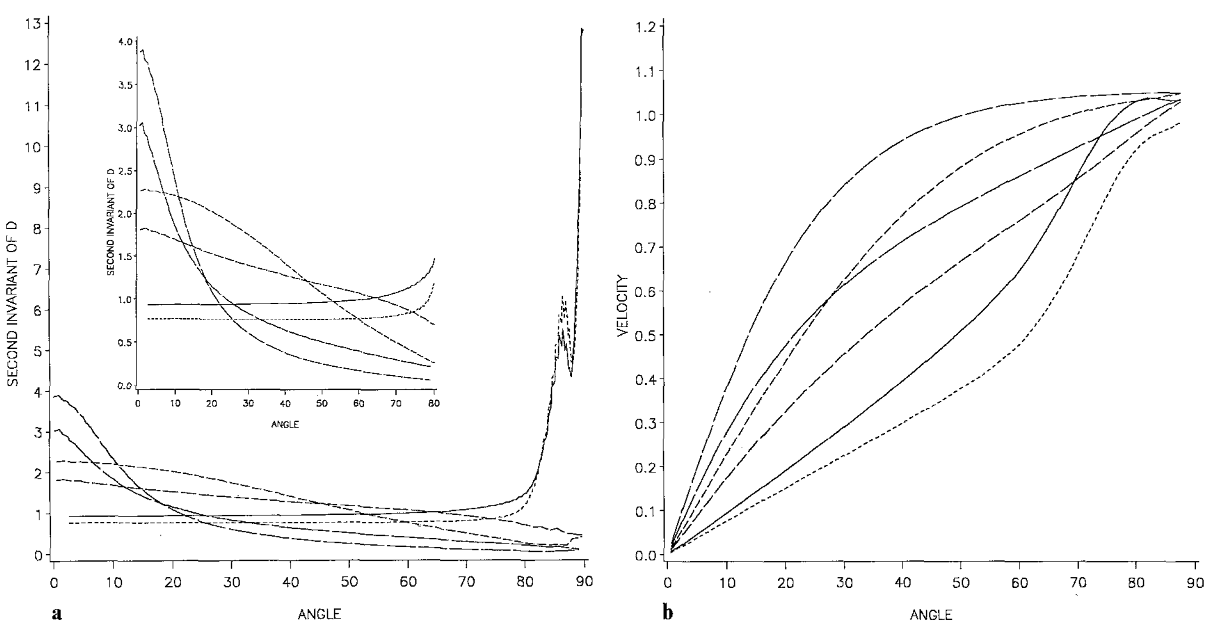

Fig. 10. Distribution of the second invariant of the strain-rate tensor and the tangential speed on the penetrator nose surface for $\alpha = 8$, both with and without the consideration of frictional forces (see Fig. 9 for the legend to the curves)

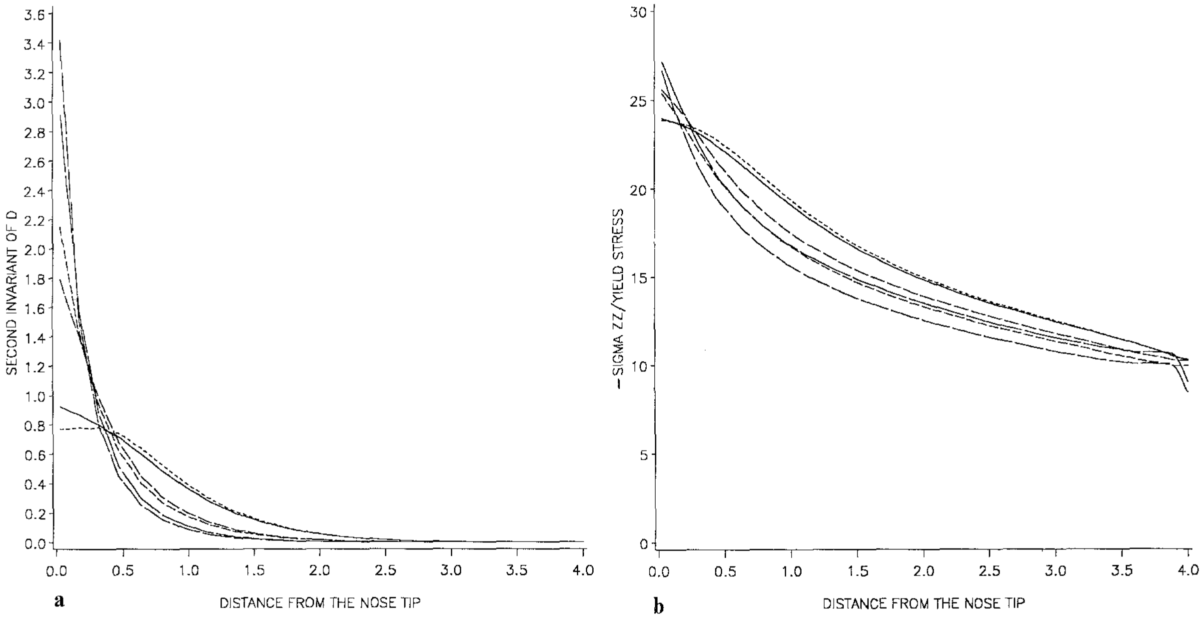

Fig. 11. Distribution of the second invariant of the strain-rate tensor and $(-\sigma_{zz})$ at points on the axial line for $\alpha = 8$, both with and without the consideration of frictional forces (see Fig. 9 for the legend to the curves)

the effect of the frictional force on the tangential speed is quite noticeable for each one of the three nose shapes. Except at the nose tip and the nose periphery, the consideration of frictional forces decreases the tangential speed at every point on the nose surface. Figure 11 depicts the decay of the second invariant I of the strain-rate tensor and $(-\sigma_{zz})$ along the axial line for the three nose shapes. For the blunt nosed penetrator, I decreases slowly as compared to the other two nose shapes, implying that the deformations of the target spread farther for the blunt nosed penetrator. For all three nose shapes, I becomes essentially zero at a point distant $2.5r_0$ from the nose tip, suggesting that severe deformations of the target material occur at points located within $2.5r_0$ from the nose surface. Thus, the target region studied is adequate, and the computed values of different field variables at points in the vicinity of the target/penetrator interface should be quite good.

4 Conclusions

We have analyzed the effect of frictional forces on the steady state deformations of a viscoplastic target being penetrated by a rigid cylindrical penetrator. It is postulated that the frictional force at a point depends upon the normal traction and the relative velocity of sliding between the two surfaces at that point. The approximate value of the parameters appearing in the expression for the friction force is found by comparing results for the penetration problem with those obtained by modelling the deforming target material as a viscous fluid and using the Karman-Pohlhausen approximation that relates the speed of the fluid in the boundary layer to that at far away points. It is found that the consideration of frictional forces affects significantly the distribution of the second-invariant of the strain-rate tensor and the tangential speed on the penetrator nose surface, but minimally the distribution of the normal traction there for each one of the three nose shapes, namely, the blunt, hemispherical, and ellipsoidal. For the blunt nosed penetrator, peak values of the second invariant of the strain-rate tensor occur at points near the nose periphery, and are considerably higher than those for the other two nose shapes, which occur at points adjacent to the nose tip.

Acknowledgements

This work was supported by the U.S. Army Research Office Contract DAAL03-89-K-0050 to the University of Missouri – Rolla. Some of the computations were performed on the NSF sponsored supercomputer center at the University of Illinois at Urbana-Champaign. We thank Dr. S. C. Lee for useful discussions regarding the boundary layer theory.

References

[1] Batra, R. C., Gobinath, T.: Steady state axisymmetric deformations of a thermoviscoplastic rod penetrating a thick thermoviscoplastic target. Int. J. Impact Eng. **11**, 1–31 (1991).
[2] Gobinath, T., Batra, R. C.: A steady state axisymmetric penetration problem for rigid perfectly plastic materials. Int. J. Eng. Sci. **29**, 1315–1331 (1991).
[3] Batra, R. C., Wright, T. W.: Steady state penetration of rigid perfectly plastic targets. Int. J. Eng. Sci. **24**, 41–54 (1986).
[4] Batra, R. C.: Steady state penetration of viscoplastic targets. Int. J. Eng. Sci. **25**, 1131–1141 (1987).
[5] Batra, R. C.: Steady state penetration of thermoviscoplastic targets. Comp. Mech. **3**, 1–12 (1988).
[6] Jayachandran, R., Batra, R. C.: Steady state penetration of elastic perfectly plastic targets. Acta Mech. **92**, 9–27 (1992).
[7] Birchoff, G., McDougall, D. P., Pugh, E. M., Taylor, G.: Explosives with lined cavities. J. Appl. Phys. **19**, 563–582 (1948).
[8] Pack, D. C., Evans, W. M.: Penetration of high velocity jets. Proc. Phys. Soc. Lond. **B64**, 298–303 (1951).
[9] Alekseevskii, V. P.: Penetration of a rod into a target at high velocity. Comb. Expl. and Shock Waves **2**, 63–66 (1966) (translation from Russian).
[10] Tate, A.: A theory for the deceleration of long rods after impact. J. Mech. Phys. Solids **15**, 387–399 (1967).
[11a] Tate, A.: Long rod penetration models. Part I. A flow field model for high speed long rod penetration. Int. J. Mech. Sci. **28**, 535–548 (1986).
[11b] Tate, A.: Long rod penetration models. Part II. Extensions to the hydrodynamic theory of penetration. Int. J. Mech. Sci. **28**, 599–612 (1986).
[12] Backman, M. E., Goldsmith, W.: The mechanics of penetration of projectiles into targets. Int. J. Eng. Sci. **16**, 1–99 (1978).
[13] Jones, G. H., Zukas, J. A.: Mechanics of penetration: analysis and experiment. Int. J. Eng. Sci. **16**, 879 (1978).
[14] Anderson, C. E., Bodner, S. R.: The status of ballistic impact modeling. Int. J. Impact Eng. **7**, 9–35 (1988).
[15] Awerbuch, J.: MED Report No. 28. Technion-Israel Inst. of Techn. 1970.
[16] Awerbuch, J., Bodner, S. R.: Analysis of the mechanics of perforation of projectiles in metallic plates. Int. J. Solids Struct. **10**, 671–684 (1974).
[17] Ravid, M., Bodner, S. R.: Dynamic perforation of viscoplastic plates by rigid projectiles. Int. J. Eng. Sci. **21**, 577–591 (1983).
[18] Ravid, M., Bodner, S. R., Holcman, I.: Analysis of very high speed impact. Int. J. Eng. Sci. **25**, 473–482 (1987).

[19] Batra, R. C., Chen, X.: An approximate analysis of steady state axisymmetric deformations of viscoplastic targets. Int. J. Eng. Sci. **28**, 1347–1358 (1990).
[20] Jones, S. E., Gillis, P. P., Foster, J. C.: On the penetration of semi-infinite targets by long rods. J. Mech. Phys. Solids **35**, 121–131 (1987).
[21] Woodward, R. L.: Penetration of semi-infinite metal targets by deforming projectiles. Int. J. Mech. Sci. **24**, 73 (1982).
[22] Forrestal, M. J., Okajima, K., Luk, V. K.: Penetration of 6061-T651 aluminium targets with rigid long rods. J. Appl. Mech. **55**, 755–760 (1988).
[23] Oden, J. T.: On the general rolling contact problem for finite deformations of a viscoelastic cylinder. Comp. Meth. Appl. Mech. Engng. **57**, 297–367 (1986).
[24] Chen, E.-P.: Penetration into dry porous rock. A numerical study on frictional simulation. In: Computational techniques for contact, impact, penetration and perforation of solids (Schwer, L. E., Salamon, N. J., Kiu, W. K., eds.), pp. 325–336. ASME Press 1989.
[25] Tate, A.: A simple hydrodynamic model for the strain field in a target by the penetration of a high speed long rod projectile. Int. J. Eng. Sci. **16**, 845–858 (1978).
[26] Schlichting, H.: Boundary-layer theory (translated by J. Kestin). New York: McGraw-Hill 1979.

Authors' address: X. Chen and R. C. Batra, Department of Mechanical and Aerospace Engineering and Engineering Mechanics, University of Missouri-Rolla, Rolla, MO 65401-0249, U.S.A.